A Speed-Sensorless FS-PTC of Induction Motors Using Extended Kalman Filters

Md. Habibullah, *Student Member, IEEE,* and Dylan Dah-Chuan Lu, *Senior Member, IEEE*

***Abstract*—A sensorless finite state predictive torque control (FS-PTC) strategy uses stator current, estimated stator and rotor flux, and estimated rotor speed to predict stator flux and torque. Direct application of measured stator currents, and using a noisy estimated speed in the prediction model degrade the steady state performance in terms of higher current total harmonic distortion (THD), torque ripple, and flux ripple, especially at low speeds. This paper proposes an extended Kalman filter (EKF), a promising state observer, based improved prediction model of sensorless FS-PTC for induction motor (IM) drives. The EKF has been used to estimate rotor speed, rotor/stator flux, and stator currents accurately. The estimated stator currents instead of measured currents are fed back to the prediction model and thus small stator current total harmonic distortion (THD) is confirmed. Depending on the commanded speed, either rotor current model or open-loop stator voltage model is proposed for the EKF to achieve better performance in a wide speed range including field weakening region. The proposed control system has been verified experimentally, and excellent torque and flux responses, robustness, and stable operation at lower and higher speeds have been achieved.**

***Index Terms*—Sensorless control, finite state predictive torque control (FS-PTC), extended Kalman filter (EKF), field weakening, induction motor (IM).**

I. Introduction

PREDICTIVE torque control (PTC) strategy is a recent alternative to the conventional direct torque control (DTC) and field orientation control (FOC) strategies. Due to its intuitive features, easy implementation, and easy inclusion of nonlinearities and constraints, PTC has widely been investigated [1]–[5]. In finite state PTC (FS-PTC), torque and stator flux are predicted for the finite number of possible switching states of a power converter. The switching state which minimizes torque and flux ripples most is finally chosen as the optimal switching state and is obtained by actuating a predefined cost function. The selected optimal switching state is directly applied to the converter to produce the voltage vector to be applied to the motor in the next sampling instant, without requiring an intermediate modulation stage [2]. Another important advantage of PTC is that it has no inner current control loop. Moreover, PTC structure is simpler compared to the classical DTC and FOC. However, compared with classic DTC and FOC, PTC produces worse stator current total harmonic distortion (THD) [6]. It is because PTC requires large computation and also uses the measured stator currents in the prediction model directly and, therefore, predictions are affected by the measurement errors and stator currents THD.

Generally, in PTC, a speed control loop is used to generate the reference torque through a proportional-integral (PI) controller [5]. The speed is measured through a speed encoder/sensor, which is mounted on the motor shaft and is expensive and less reliable. Moreover, the encoder requires speed measurement card and other necessary software. Hence, induction motor (IM) drives without a speed sensor are attractive due to their lower cost and higher reliability [7]. Unfortunately, to date, very few works on sensorless FS-PTC have been published. The speed sensor must be avoided to get the control system widely accepted by different industry applications. When a speed sensor from the PTC is removed, rotor speed must be estimated through proper design of observer using measurements of stator voltages and currents.

Many speed observers have been proposed in the past years, such as full-order and reduced-order observers, model reference adaptive system (MRAS) observer [8], sliding mode observer (SMO) [9], Luenberger observer [10], extended Kalman filter (EKF) [11], [12], etc. In [10], an exact speed estimation model is proposed to operate the machine in the field weakening region by using Luenberger observer to overcome the sampled data modeling error. But the current controller introduces instability at the lower speeds. Among all the aforementioned strategies, reduced-order SMO is the simplest one, but its robustness and estimation accuracy is not satisfactory. In order to compensate the estimation error, a compensated voltage model is proposed in [8], [13]; however, it requires actual inverter parameters, and additional controllers to avoid offset and drift problems. Thus, the estimation accuracy of SMO is only fair, and the controller suffers from chattering noise. Recently, PTC has been implemented without speed encoder for motor drives applications [9], [13]–[15]. In [13], an encoderless FS-PTC has been proposed with a compensated MRAS observer. The robustness of the system is confirmed by estimating the stator resistance online. However, THDs of the stator currents are very high at lower speeds, and the control performance is greatly affected by the noisy estimated speed. To improve the low-speed performance, another encoderless PTC is proposed in [15] with a revised prediction model and a full-order sliding mode observer (FOSMO). The speed dependence of the prediction and observer models is

Manuscript received November 20, 2014; revised February 18, 2015 and April 23, 2015; accepted May 13, 2015.

M. Habibullah is with the School of Electrical and Information Engineering, The University of Sydney, Sydney, N.S.W. 2006, Australia (e-mail:md.habibullah@sydney.edu.au).

D.D.C. Lu is with the School of Electrical and Information Engineering, The University of Sydney, Sydney, N.S.W. 2006, Australia (e-mail:dylan.lu@sydney.edu.au).

avoided, and satisfactory speed response is achieved even though the estimated speed is still noisy. However, the observer is greatly influenced by the stator resistance variation and produces oscillations in torque and flux responses. In both aforementioned study, the stability of the controller at very low and high speeds i.e., field weakening have not been addressed. Moreover, to date, all previous studies on PTC with speed sensor or without speed sensor use the measured stator currents directly at prediction stage. Direct use of these measured currents leads to undesired switching actuation, and worsens the stator currents. As a consequence, the controller produces high current THD, especially at lower speeds.

Extended Kalman filter (EKF) is a promising optimization observer because of the robustness against parameter uncertainties [11], [12], [16]–[19], and many sensorless problems have been successfully solved with it. The observer basically deals with linearization of the nonlinear discrete model of IM using the present estimated states and available inputs [12]. It can estimate the speed from zero to nominal speed accurately. Recently, EKF is proposed for FS-PTC in [20] to estimate the speed accurately. But only simulation results are presented to show its effectiveness. However, EKF requires more calculations, which limits the sampling frequency. Nevertheless modern digital signal processors (DSPs) can easily solve this problem due to the high computational power. To estimate the speed, EKF automatically estimates the other states such as stator currents and flux, without further increasing the computational burden. Using these states, the prediction model in FS-PTC can avoid the measurement noises and reduce the current THD. It results improved transient and steady state stator flux and torque responses. Hence, it is expected to be facilitated the attainment of full benefits of FS-PTC using EKF.

The performance of FS-PTC is greatly affected by the speed estimation error and the currents measurement noises, especially at low speeds. In this paper, an accurate prediction model is proposed by estimating the rotor speed and stator currents using EKF. In order to avoid the currents measurement noises, the estimated stator currents instead of measured currents are fed back to the prediction model. The stator currents THDs are reduced and thus improved speed, torque and flux responses are achieved. The proposed control system is also robust against stator resistance variations. To reduce the speed error in a wide speed range, both current and open-loop voltage models of IM are proposed for EKF. Taking into account stator currents "$\left(\vec{i}_{s\alpha},\ \vec{i}_{s\beta}\right)$", rotor/stator flux "$\left(\vec{\psi}_{\alpha},\ \vec{\psi}_{\beta}\right)$", rotor speed "$\omega_m$", and load torque "$T_l$" as states, sixth-order nonlinear discrete model of IM is considered. The proposed control system has been carried out experimentally, and good performance in terms of torque and flux responses, robustness, speed accuracy, and stability at low and high speeds including field weakening region has been achieved.

The remaining parts of the paper are organized as follows: Section II provides mathematical models of IM. Section III presents a brief description of the proposed control strategy. Field weakening operation of the proposed sensorless drive is discussed briefly in section IV. Simulation results are provided in section V. The experimental setup and the experimental results are discussed in sections VI and VII, respectively. Finally, the paper is concluded in section VIII.

II. Induction motor model

The state space model of IM is described in a stationary reference frame (α, β), and can be expressed by the following equations (1)–(6):

$$\vec{v}_s = R_s\vec{i}_s + \frac{d\vec{\psi}_s}{dt} \tag{1}$$

$$0 = R_r\vec{i}_r + \frac{d\vec{\psi}_r}{dt} - j\omega_e\vec{\psi}_r \tag{2}$$

$$\vec{\psi}_s = L_s\vec{i}_s + L_m\vec{i}_r \tag{3}$$

$$\vec{\psi}_r = L_m\vec{i}_s + L_r\vec{i}_r \tag{4}$$

$$T_e = 1.5p\Im m\left\{\vec{\psi}_s^* \cdot \vec{i}_s\right\} \tag{5}$$

$$J\frac{d\omega_m}{dt} = T_e - T_l \tag{6}$$

where $\vec{v}_s$ is the stator voltage vector, $\vec{i}_s$ is the stator current vector, $\vec{i}_r$ is the rotor current vector, $\vec{\psi}_s$ is the stator flux vector, $\vec{\psi}_r$ is the rotor flux vector, T_e is the electromagnetic torque, T_l is the load torque, ω_m is the rotor angular speed, ω_e is the rotor angular frequency, *p* is the number of pole pairs, and the others are the system parameters.

The dynamic model of IM accounts stator current $\vec{i}_s$, and flux $\vec{\psi}$ (either $\vec{\psi}_s$ or $\vec{\psi}_r$) as state variables [19]. For rotor speed ω_m estimation, the speed is to be treated as an additional state variable, and it is directly related to the rotor angular frequency ω_e by the number of pole pairs *p* as

$$\omega_e = p\omega_m. \tag{7}$$

The load torque T_l is taken into account as a state variable to improve the speed estimation accuracy at very low speeds. For simplicity, since the sampling time is too short compared with the desired torque response, it is a common practice to assume the derivative of the load torque $\dot{T}_l = 0$ [11], [19]. Therefore, rearranging (1)–(7), the extended sixth-order nonlinear state space model of IM can be expressed as follows:

$$\dot{x} = f(x,u) \tag{8}$$

where, for rotor current model (CM),

$$x = \left[\vec{i}_{s\alpha}\ \vec{i}_{s\beta}\ \vec{\psi}_{r\alpha}\ \vec{\psi}_{r\beta}\ \omega_m\ T_l\right]^T$$

$$u = [\vec{u}_{s\alpha}\ \vec{u}_{s\beta}]^T$$

$$f(x,u) = \begin{pmatrix} -\left(\frac{R_s}{L_\sigma} + \frac{L_m^2R_r}{L_\sigma L_r^2}\right)\vec{i}_{s\alpha} + \frac{L_mR_r}{L_\sigma L_r^2}\vec{\psi}_{r\alpha} + \frac{L_m\omega_e}{L_\sigma L_r}\vec{\psi}_{r\beta} + \frac{\vec{u}_{s\alpha}}{L_\sigma} \\ -\left(\frac{R_s}{L_\sigma} + \frac{L_m^2R_r}{L_\sigma L_r^2}\right)\vec{i}_{s\beta} - \frac{L_m\omega_e}{L_\sigma L_r}\vec{\psi}_{r\alpha} + \frac{L_mR_r}{L_\sigma L_r^2}\vec{\psi}_{r\beta} + \frac{\vec{u}_{s\beta}}{L_\sigma} \\ \frac{L_mR_r}{L_r}\vec{i}_{s\alpha} - \frac{R_r}{L_r}\vec{\psi}_{r\alpha} - \omega_e\vec{\psi}_{r\beta} \\ \frac{L_mR_r}{L_r}\vec{i}_{s\beta} + \omega_e\vec{\psi}_{r\alpha} - \frac{R_r}{L_r}\vec{\psi}_{r\beta} \\ -\frac{3}{2}\frac{p}{J}\frac{L_m}{L_r}\vec{\psi}_{r\beta}\vec{i}_{s\alpha} + \frac{3}{2}\frac{p}{J}\frac{L_m}{L_r}\vec{\psi}_{r\alpha}\vec{i}_{s\beta} - \frac{T_l}{J} \\ 0 \end{pmatrix}$$

and, for stator voltage model (VM),

$$x = \left[\vec{i}_{s\alpha}\ \vec{i}_{s\beta}\ \vec{\psi}_{s\alpha}\ \vec{\psi}_{s\beta}\ \omega_m\ T_l\right]^T$$

$$u = [\vec{u}_{s\alpha}\ \vec{u}_{s\beta}]^T$$

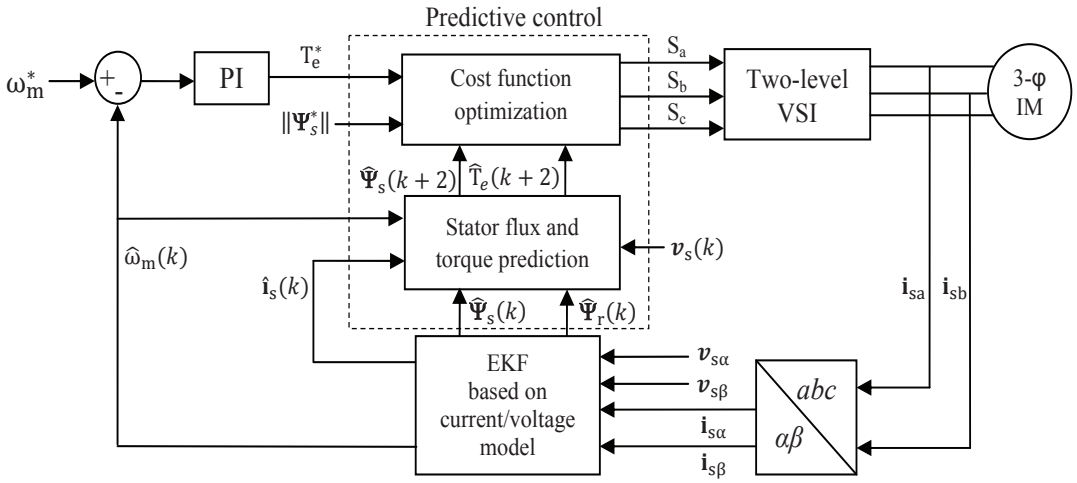

Fig. 1. Sensorless FS-PTC based IM drive.

$$f(x,u)=\begin{pmatrix} -\left(\frac{R_s}{L_\sigma}+\frac{R_rL_s}{L_\sigma L_r}\right)\vec{i}_{s\alpha}-\omega_e\vec{i}_{s\beta}+\frac{R_r}{L_\sigma L_r}\vec{\psi}_{s\alpha}+\frac{\omega_e}{L_\sigma}\vec{\psi}_{s\beta}+\frac{\vec{u}_{s\alpha}}{L_\sigma} \\ -\omega_e\vec{i}_{s\alpha}-\left(\frac{R_s}{L_\sigma}+\frac{R_rL_s}{L_\sigma L_r}\right)\vec{i}_{s\beta}-\frac{\omega_e}{L_\sigma}\vec{\psi}_{s\alpha}+\frac{R_r}{L_\sigma L_r}\vec{\psi}_{s\beta}+\frac{\vec{u}_{s\beta}}{L_\sigma} \\ R_s\vec{i}_{s\alpha}+\vec{u}_{s\alpha} \\ R_s\vec{i}_{s\beta}+\vec{u}_{s\beta} \\ -\frac{3}{2}\frac{p}{J}\vec{\psi}_{s\beta}\vec{i}_{s\alpha}+\frac{3}{2}\frac{p}{J}\vec{\psi}_{s\alpha}\vec{i}_{s\beta}-\frac{T_l}{J} \\ 0 \end{pmatrix}$$

where $\sigma = 1 - L_m^2/L_sL_r$ is the total leakage factor, and $L_\sigma = \sigma L_s$ is the leakage inductance.

III. Sensorless FS-PTC model

In a conventional sensorless FS-PTC based drive, the rotor current model of IM is considered to estimate the rotor flux, and the voltage model is considered to predict the stator flux and the torque. The estimated speed is fed back to the controller. The speed is also compared with a reference speed, and the error is processed through a PI controller to generate the reference torque. For speed sensorless drive, current model based estimator can not estimate the speed accurately at very low speeds. It is because the stator currents start to lose rotor information when the speed approaches zero and cease completely at zero speed. On the other hand, voltage model based estimator can estimate any speed from zero to rated speed. But open-loop voltage model based stator flux is not good enough for the controller, and the estimator becomes unstable at higher speeds due to some problems such as dc offset, drifts, and more parameter sensitivity. These problems can be compensated but not fully unavoidable resulting in complex PTC structure. This is why, in compared with current model, voltage model produces more steady state torque and flux ripples. However, for better speed response, open-loop voltage model can be used at lower speeds to estimate rotor speed and stator flux directly without compensating the aforementioned negative effects. This will cost a bit higher torque and flux ripples which are acceptable for lower speeds considering improved speed response. In this paper, for the reference speed $\omega_m^* > \pm$60rpm ($\pm$2Hz), the rotor model based EKF is used to estimate the rotor speed and the rotor flux, otherwise, the voltage model based EKF is used to estimate the rotor speed and the stator flux. Measurement noises and harmonics in the stator currents are also filtered out through EKF, and the estimated currents are fed back to the controller. Fig. 1 presents the overall control diagram of the proposed sensorless FS-PTC, which mainly includes three parts: EKF for rotor/stator flux estimation, stator flux and torque prediction, and cost function optimization (voltage vector selection).

A. EKF for rotor/stator flux estimation

The extended model of IM in either CM or VM, depends on the reference speed, is used in EKF to estimate the rotor/stator flux. Since the EKF is an optimal state estimator based on stochastic uncertainties of the system variables, two different white noises are injected into the system model: one is process noise, and the other one is measurement noise. The sixth-order nonlinear extended model of IM for EKF can be expressed as [17]:

$$\dot{x} = f(x,u) + w(t) \quad (System) \tag{9}$$

$$y = Cx + v(t) \quad (Measurement) \tag{10}$$

where C is the model output matrix, $w(t)$ is the process noise, and $v(t)$ is the measurement noise. The covariance matrices of $w(t)$ and v(t) are Q and R, respectively.

Therefore, C, Q and R can be expressed as

$$C = \begin{bmatrix} 1 & 0 & 0 & 0 & 0 & 0 \\ 0 & 1 & 0 & 0 & 0 & 0 \end{bmatrix} \tag{11}$$

$$Q = cov(w) = E\left\{ww^T\right\} \tag{12}$$

$$R = cov(v) = E\left\{vv^T\right\}. \tag{13}$$

The continuous model in (9) and (10) is discretized for the implementation of EKF using standard forward-Euler approximation by

$$\frac{d\mathbf{x}}{dt} \approx \frac{\mathbf{x}(k+1) - \mathbf{x}(k)}{T_s} \tag{14}$$

where T_s is the sampling time, and $\mathbf{x}(k)$ and $\mathbf{x}(k+1)$ are present and next states of the system, respectively.

The recursive form of the EKF, including stochastic uncertainties, may be expressed by the following system of equations [18].

Prediction process:

$$\hat{x}[k|k-1] = \hat{x}[k-1|k-1] + f\left(\hat{x}[k-1|k-1], u[k]\right) T_s \quad (15)$$

$$P[k|k-1] = \frac{\partial f\left(x[k], u[k]\right)}{\partial x[k]} P[k|k] \frac{\partial f\left(x[k], u[k]\right)}{\partial x[k]}^T + Q \quad (16)$$

where $\hat{x}$ is the state estimate, P is the state estimate error covariance matrix, and $\frac{\partial f}{\partial x}|_{\hat{x}[k],\hat{u}[k]}$ is the corresponding Jacobian matrix which involves linearization of nonlinear state space model of IM. For simplicity, all covariance matrices are assumed to be diagonal [18]. The diagonal elements are tuned in MATLAB/Simulink environment using a trial and error method.

Kalman gain:

$$K\left[k\right] = P[k|k-1]C^T\left(CP[k|k-1]C^T + R\right)^{-1} \quad (17)$$

Innovation process:

$$\hat{x}[k|k] = \hat{x}[k|k-1] + K[k]\left(y[k] - C\hat{x}[k|k-1]\right) \quad (18)$$

$$P[k|k] = P[k|k-1] - K[k]CP[k|k-1] \quad (19)$$

The predictions in (15) and (16) are updated with the present measurements by (18) and (19) using the Kalman gain calculated in (17).

After estimating the rotor/stator flux using EKF, the other flux (stator/rotor) is calculated using the following simple relationship between stator and rotor flux:

$$\vec{\hat{\psi}}_s = \frac{L_m}{L_r}\vec{\hat{\psi}}_r + \sigma L_s \vec{\hat{i}}_s \quad (20)$$

where $\vec{\hat{i}}_s$ is the estimated stator current. Equation (20) says stator flux performance is greatly affected by the quality of the stator currents. If the stator currents contain measurement noise or harmonics, it will produce ripple in the estimated stator flux which expedites the wrong actuation of voltage vectors, yielding poorer speed and torque responses.

B. Prediction of stator flux and torque

Knowing $\vec{\hat{\psi}}_s(k)$ and using standard forward-Euler approximation (14), the magnitude of the stator flux and the torque at the instant $(k+1)$ can be predicted as

$$\vec{\hat{\psi}}_s(k+1) = \vec{\hat{\psi}}_s(k) + T_s\vec{v}_s(k) - T_sR_s\vec{\hat{i}}_s(k) \quad (21)$$

$$\vec{i}_s(k+1) = \left(1 + \frac{T_s}{\tau_\sigma}\right)\vec{\hat{i}}_s(k) + \frac{T_s}{(\tau_\sigma + T_s)} \left\{\frac{1}{R_\sigma}\left[\left(\frac{k_r}{\tau_r} - k_r j\hat{\omega}_e\right)\vec{\hat{\psi}}_r(k) + \vec{v}_s(k)\right]\right\} \quad (22)$$

$$\hat{T}_e(k+1) = 1.5p\Im m\left\{\vec{\hat{\psi}}_s(k+1)^* \cdot \vec{i}_s(k+1)\right\} \quad (23)$$

where $\hat{\omega}_e = p\hat{\omega}_m$ is the estimated rotor angular frequency, $k_r = L_m/L_r$ is the rotor coupling factor, $R_\sigma = R_s + k_r^2 R_r$ is the equivalent resistance referred to stator, $\tau_\sigma = L_\sigma/R_\sigma$ is the transient time stator constant, and $\tau_r = L_r/R_r$ is the rotor time constant.

It is evident that stator current (22) and torque (23) predictions are greatly affected by the speed estimation error. Therefore, in this paper, the speed is estimated accurately and, an improved prediction model is achieved.

C. Voltage vector selection

The optimal voltage vector is selected based on the traditional PTC [5] which includes two steps: torque and flux prediction and cost function optimization, as shown in Fig. 1. State-space model of IM for estimation and prediction of the states, and a priority based cost function for actuation are used to select the optimal voltage vector. Priority is given on stator flux in compared with the torque. The cost function can be expressed as

$$g = \left|T_e^*(k+1) - \hat{T}_e(k+1)\right| + \lambda_\psi\left|\left|\vec{\psi}_s^*\right| - \left|\vec{\hat{\psi}}_s(k+1)\right|\right| \quad (24)$$

where $T_e^*(k+1)$ is the reference torque and $\hat{T}_e(k+1)$ is the predicted torque for a given switching state, $\vec{\psi}_s^*$ is the reference stator flux and $\vec{\hat{\psi}}_s(k+1)$ is the predicted stator flux, and λ_ψ is the weighting factor which sets the importance of stator flux in compared with the torque. The reference stator flux $\vec{\psi}_s^*$ is constant for all time. Since the sampling frequency is too high compared with the probability of load change over the control duration, which is too short, it is a general practice to assume $T_e^*(k) = T_e^*(k+1)$.

In a two-level voltage source inverter (2L-VSI), there are eight possible switching states and the state which minimizes g most is selected for the next step to produce the voltage vector to be applied to the motor.

In a real time implementation, calculation time of control algorithm introduces a time delay which must be compensated [21]. It is done by two-step ahead prediction considering $\vec{\hat{\psi}}_s(k+1)$ and $\vec{i}_s(k+1)$ as initial conditions for the predictions at instant $k+2$. Since the frequency of the rotor flux is too low compared with the sampling frequency, the rotor flux $\vec{\hat{\psi}}_r(k)$ and $\vec{\hat{\psi}}_r(k+1)$ are assumed to be same. Hence, to implement the delay compensation scheme, the predicted stator flux and the torque at instant $k+2$ are obtained by

$$\vec{\hat{\psi}}_s(k+2) = \vec{\hat{\psi}}_s(k+1) + T_s\vec{v}_s(k+1) - T_sR_s\vec{\hat{i}}_s(k+1) \quad (25)$$

$$\vec{i}_s(k+2) = \left(1 + \frac{T_s}{\tau_\sigma}\right)\vec{i}_s(k+1) + \frac{T_s}{(\tau_\sigma + T_s)} \left\{\frac{1}{R_\sigma}\left[\left(\frac{k_r}{\tau_r} - k_r j\hat{\omega}_e\right)\vec{\hat{\psi}}_r(k+1) + \vec{v}_s(k+1)\right]\right\} \quad (26)$$

$$\hat{T}_e(k+2) = 1.5p\Im m\left\{\vec{\hat{\psi}}_s(k+2)^* \cdot \vec{i}_s(k+2)\right\}. \quad (27)$$

Now, considering the calculation delay in real time implementation, the cost function to minimize is

$$g = \left|T_e^*(k+2) - \hat{T}_e(k+2)\right| + \lambda_\psi\left|\left|\vec{\psi}_s^*\right| - \left|\vec{\hat{\psi}}_s(k+2)\right|\right|. \quad (28)$$

In order to protect over current through the stator, the cost function g must include a third term I_m which is designed on

the basis of maximum allowable current through the machine. If the absolute value of predicted current $|\vec{i}_s(k+2)|$ for any particular switching state is higher than the maximum current, then that particular switching state will be canceled by setting a higher value against I_m. Therefore, the term I_m can be defined as

$$I_m = \begin{cases} \infty, & \text{if } |\vec{i}_s(k+2)| > i_{max} \\ 0, & \text{otherwise.} \end{cases}$$

Here, i_{max} is the maximum current rating of the IM.

Thus, the complete cost function g for the controller is

$$g = \left|T_e^*(k+2) - \hat{T}_e(k+2)\right| + \lambda_\psi \left| \left|\vec{\psi}_s^*\right| - \left|\vec{\hat{\psi}}_s(k+2)\right| \right| + I_m. \tag{29}$$

IV. Proposed sensorless FS-PTC in the field weakening region

For high speed applications, such as ac servo, gearless traction drives, and spindle drives, the machine requires to operate in the field weakening region [10], [22]–[24]. For maximum torque capability of the machine in the field weakening region, the required voltage $\vec{v}_{s,req}$ and stator current $\vec{i}_{s,req}$ are equal to their maximum values. However, the maximum voltage and stator current to be applied to the machine terminal are limited by the available inverter output voltage V_{max} and inverter current rating I_{max}. Along with dc link voltage, the inverter output voltage is also dependent on the used modulation strategy. For instance, maximum voltage V_{max} of pulse width modulation (PWM) with space vector modulation (SVM) strategy is $V_{dc}/\sqrt{3}$ [25]. Since, FS-PTC strategy directly applies the switching signals to the inverter without any intermediate modulation stage, the maximum available voltage V_{max} is $2/3V_{dc}$. If the required voltage and current to drive the machine in the field weakening region are $\vec{v}_{s,req}$ and $\vec{i}_{s,req}$, respectively, the limit conditions of the control system can be represented by the following inequalities:

$$\vec{v}_{s,req} \leq V_{max} \tag{30}$$

$$\vec{i}_{s,req} \leq I_{max}. \tag{31}$$

In this study, the inverter current rating is higher than the machine current rating. Hence, I_{max} is set equal to the maximum current rating i_{max} of the motor.

The voltage drop across the stator resistance at high speed (above base speed) is negligible. Hence, modifying (1) with the rotor speed dependent back emf i.e., $\frac{d\vec{\psi}_s}{dt} = \omega_e \psi_s$, the required maximum voltage $\vec{v}_{s,req}$ in the field weakening region can be approximated as

$$\vec{v}_{s,req} \cong \sqrt{2}\hat{\omega}_e |\vec{\hat{\psi}}_s|. \tag{32}$$

In the proposed FS-PTC, for time delay implementation, $|\vec{\hat{\psi}}_s|$ in (32) will be replaced by the absolute value of $\vec{\hat{\psi}}_s(k+1)$ from (21).

The total dynamic operation of the machine can be divided into three speed regions: region I, region II, and region III, namely, constant torque region, constant power region, and reduced power region, respectively. The regions II and III are basically field weakening regions. In region I, the torque remains at maximum value, provided that the stator current and the stator flux are maximum. Region II starts when $\vec{v}_{s,req} \geq V_{max}$, and the stator flux starts to decrease to keep the back emf nearly constant. But the stator current continues to remain at its rated value to ensure the maximum torque capability of the machine. Since the torque reduces with increasing speed, the power delivered to the load in the region II is approximately constant. If the speed increases further, at a particular point, the maximum available voltage V_{max} can not inject the required stator current and the current starts to decrease; the point is the starting point of region III. The power delivered to the load in the region III decreases as the speed increases.

When the speed of the machine enters into the field weakening region, the reference stator flux which is constant in the FS-PTC should be changed. In this paper, the new reference stator flux $\vec{\psi}_{s,new}^*$ is obtained by the conventional $1/\omega_r$ method [10], [26], where ω_r is the rotor speed. In this method, the stator flux reference is changed in proportion to the inverse of rotor speed. The base speed of the machine ω_b, the estimated speed $\hat{\omega}_e$ as the control scheme is sensorless, and the rated stator flux $\vec{\psi}_s^*$ are used to determine $\vec{\psi}_{s,new}^*$, and the relationship among them can be expressed as

$$\vec{\psi}_{s,new}^* = \frac{\omega_b}{\hat{\omega}_e} |\vec{\psi}_s^*|. \tag{33}$$

The new reference stator flux $\vec{\psi}_{s,new}^*$ will be used in (29) replacing the rated stator flux reference $|\vec{\psi}_s^*|$. The weighting factor λ_ψ in (29) will also be adjusted. Hence, the new cost function for the field weakening operation can be expressed as

$$g = \left|T_e^*(k+2) - \hat{T}_e(k+2)\right| + \lambda_{\psi,new} \left| \left|\vec{\psi}_{s,new}^*\right| - \left|\vec{\hat{\psi}}_s(k+2)\right| \right| + I_m \tag{34}$$

where $\lambda_{\psi,new}$ is the new weighting factor.

It is well known that the expected maximum torque in the field weakening region is a consequence of the voltage and current limit. To achieve maximum torque, conventionally, a current controller injects maximum available torque producing component of stator current maintaining the current limit (31). In order to avoid the instability of the machine at very high speeds, a predefined limit of flux producing component of stator current is also used in the controller [24].

In the FS-PTC, as already mentioned in the section-III, the required voltage vector is predicted by minimizing torque and flux tracking errors, and the reference torque is generated by anti-windup mechanism. Hence, for a certain level of stator flux, the selected voltage vector will always produce possible maximum torque. If the reference torque is too high, the required stator current can exceed the current limit (31). It will be maintained automatically by the term I_m in (34), thus no additional current controller is required.

V. Simulation results

In order to verify the effectiveness of the proposed sensorlessless FS-PTC strategy, some simulation tests are carried out in MATLAB/Simulink environment. The parameters of the IM used for simulation are listed in

TABLE I
INDUCTION MOTOR PARAMETERS

$R_s = 47.9\Omega$	$L_m = 2.437H$	$\psi_{snom} = 0.85Wb$
$R_r = 37.8\Omega$	$N_p = 2$	$T_{nom} = 1.0Nm$
$L_s = 2.631H$	$J = 0.001Kg.m^2$	$P = 175W$
$L_r = 2.631H$	$\omega_m = 1382rpm$	$i_{s,rms} = 0.46A$

TABLE II
CONTROLLER AND LOAD PARAMETERS

Controller parameters	Load parameters
$k_p = 0.125$	$T_{nom} = 3Nm$
$k_i = 1.376$	$P = 175W$
$\lambda_\psi = 5, \lambda_{\psi,new} = 2$	$\omega = 2500rpm$
$i_{max} = 0.65A$	Friction torque=0.15Nm @ 1500rpm

Table I, and the controller and the load parameters are listed in Table II. The optimized voltage vector is produced by using a 2L-VSI. The inverter is characterized by a dc link voltage of 586V. For estimation, prediction, and actuation of the objective function, a sampling time is set to $130\mu s$. The gain coefficients of the PI speed control loop have been set considering the bandwidth of 20Hz and the phase margin of $85°$. In the EKF algorithm, the initial values of states and the diagonal elements of covariance matrices have been set as $\hat{X}(0) = [0;\ 0;\ 0;\ 0;\ 0;\ 0]$, $P(0) = 10^{-7} * diag([1\ 1\ 1\ 1\ 1\ 1], 0)$, $Q = diag([0.01\ \ 0.01\ \ 0.0001\ \ 0.0001\ \ 0.005\ \ 0.01], 0)$, and $R = diag([10\ \ 10], 0)$. The sequence of elements in covariance matrices are same as the sequence of states in the machine model. In the simulation results, actual state means the state calculated by the discrete current model of the IM.

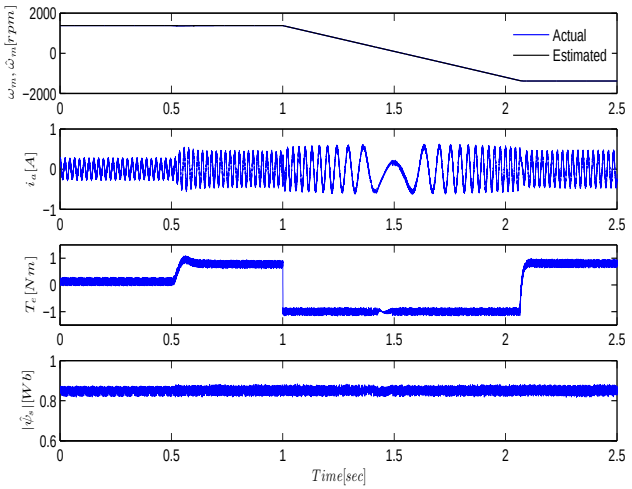

Fig. 2. Simulation results of speed, stator current, estimated torque, and stator flux at rated speed reversal and load change conditions.

The simulated results present the dynamic responses of sensorless FS-PTC system at rated speed (1382rpm) reversal condition, as shown in Fig. 2. From top to bottom, the curves are actual and estimated speed, stator current, estimated electromagnetic torque, and estimated stator flux, respectively. The stator flux is set to the nominal value at 0.85Wb which is constant. It is seen that the estimator can track the speed, the stator flux, and the load torque properly in both directions of operating frequency. Fig. 2 also shows that the stator flux is producing very good sinusoidal stator current and torque waveforms. Since the stator flux is constant with the change of load torque, a complete decoupled control of torque and flux is achieved. In order to verify the robustness of the system against load disturbance, initially, the load torque is set to 0.25Nm, then it is suddenly changed to 0.8Nm at 0.5s. It is seen that there is no transient in the stator current and stator flux. Thus, high-performance torque control is achieved.

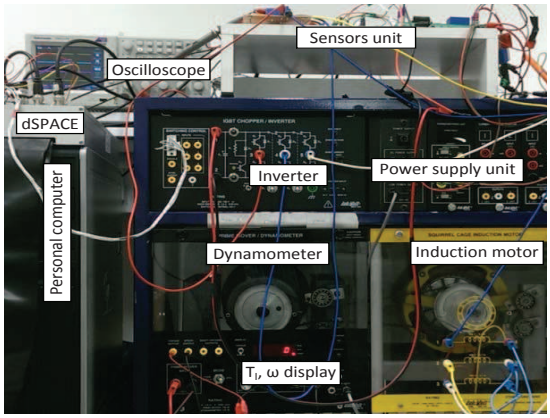

Fig. 3. Experimental setup.

VI. EXPERIMENTAL SETUP

The proposed sensorless control system is implemented in the laboratory. The setup is composed by a squirrel-cage IM driven by an IGBT based 2L-VSI of 1.1KVA with maximum current rating of 1.5A peak. A dc machine with integrated torque and speed display is coupled to the motor shaft by timing belt. The control algorithm is implemented using dSPACE DS1104 R&D controller board with ControlDesk and MATLAB Simulink software packages. For safety reasons, the inverter is characterized by a dc link voltage of 400V. Hence, the machine can not be tested with rated speed at nominal load. The sampling time similar to simulation is set to 130μs. All other system parameters are also same as those of simulation. The experimental setup is shown in Fig. 3.

For verification purposes, an incremental encoder with 2500ppr is used to measure the actual speed, and it is realized by the dSPACE 1104. The output of the encoder is sampled in every $4ms$ in order to reduce the quantization error and, therefore, for better realization of the measured speed.

Two current sensors and one voltage sensor are used to measure the stator currents and dc link voltage, respectively. The output offsets of current and voltage sensors are determined using dSPACE and ControlDesk software. Then, the offsets are compensated by subtracting those values directly from the measured stator currents and dc link voltage before feedback to the controller.

The machine is operated in two modes: normal and field weakening. For field weakening operation, the dc machine is disconnected, and tests have been carried out with only inertial

of the motor. In order to maintain the speed limit of the test setup, a reduced dc link voltage of 300V which is 51.19% of the rated voltage is applied to the inverter. Hence, the new base speed will be about 760rpm. The speed of the test setup is limited to 400% of the new base speed. In order to avoid the instability at very high speed, in this study, the stator flux is limited to 21%–100% of the rated stator flux.

The diagonal elements of covariance matrices of EKF used in the simulation are slightly adjusted for the experiments. The new covariance matrices are $Q = diag([0.5\ \ 0.5\ \ 0.0001\ \ 0.0001\ \ 0.1\ \ 0.01], 0)$ and $R = diag([1\ \ 1], 0)$. The initial state estimate error covariance matrix P(0), and the initial values of state's X(0) are considered similar as simulation. The covariance matrices remain same for both CM and VM.

VII. Experimental Results

At first the effects of current measurement noises and harmonics on the prediction model are observed. Fig. 4 depicts the improvement in torque and flux ripples due to the use of estimated stator current in the prediction model when the machine is operating at 100rpm with 25% of the nominal load torque. It is worth noting that the current THD is reduced from 2.82% to 2.01%, thus the torque and flux ripples are reduced significantly. The current THD is computed with 13 cycles of the stator current up to twenty times of its fundamental frequency using MATLAB Powergui. The steady

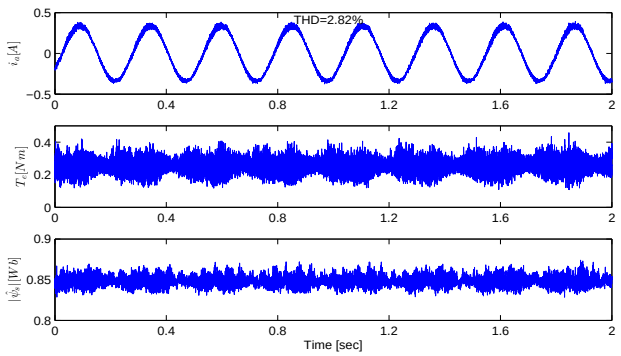

(a)

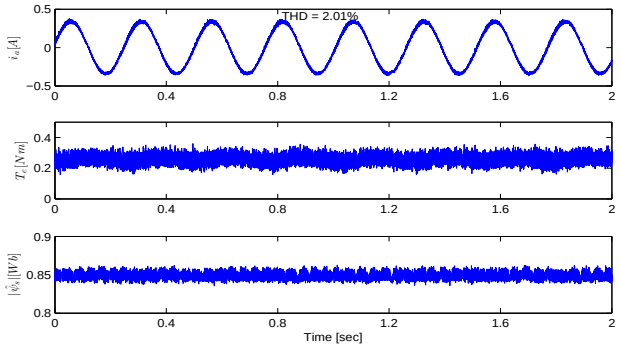

(b)

Fig. 4. Experimental steady state waveforms of stator current, estimated torque, and estimated stator flux using (a) measured and (b) estimated stator current in the prediction model.

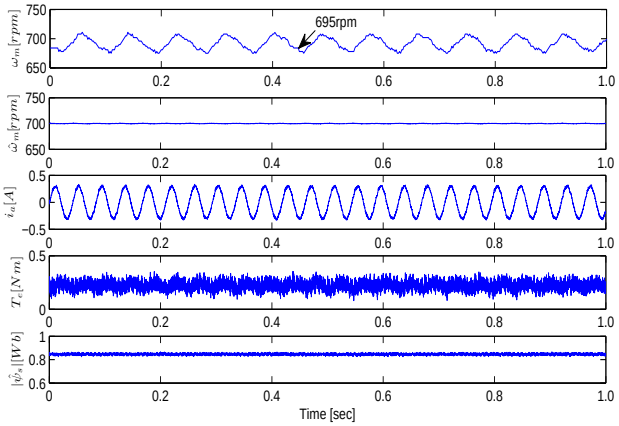

Fig. 5. Experimental steady state waveforms of measured speed, estimated speed, stator current, torque, and flux at 700rpm with 25% of the nominal load.

state behavior of the control system at 700rpm with 25% of the nominal load is presented in Fig. 5. From top to bottom, the waveforms are measured speed, estimated speed, stator current, electromagnetic torque, and stator flux, respectively. The average steady state speed error $\Delta\omega$, which is calculated by $(\hat{\omega}-\omega_m)/\hat{\omega}\times 100\%$, is about 0.7%, and the estimated speed is completely noise free. The average speed is determined by using ControlDesk software and also confirmed by observing the speed on integrated LED display. The calculated stator current THD is 4.98%. It is also seen that the stator flux produces a very good sinusoidal current waveform, yielding improved torque response.

Fig. 6 illustrates the dynamic behavior of the machine at the rated speed (1382rpm) reversal condition with a load torque of 0.35Nm. The experimental results are similar to the simulated results. The average steady state speed error is about 0.5%, and the estimated speed is free from noise. It is seen that the stator flux produces very good sinusoidal stator current and torque waveforms. The stator current THD is 7.72% at steady state condition. However, a very small deviation of stator flux magnitude is evident during speed reversal. This is not the coupling effect between torque and flux. It is because of less dc link voltage. It can be verified from the simulated results where full dc link voltage is applied to the machine, and there is no dip in the stator flux waveform.

In order to test the dynamics of the proposed sensorless FS-PTC, the torque step response from 0.25Nm to 1.0Nm is observed, and presented in Fig. 7. The torque step is achieved by changing the speed suddenly from 100rpm to rated 1382rpm. The settling time of the torque response is $1ms$, as shown by dashed line in Fig. 7, which is excellent. Thus, the proposed sensorless FS-PTC preserves the fast dynamic behavior of the basic DTC. The robustness of the proposed sensorless control system is tested by changing the load torque suddenly from 0.25Nm to full-load 1.0Nm, and the waveforms are presented in Fig. 8. From top to bottom, the waveforms are stator current, estimated speed, estimated torque, and estimated stator flux, respectively. The calculated THDs of stator current

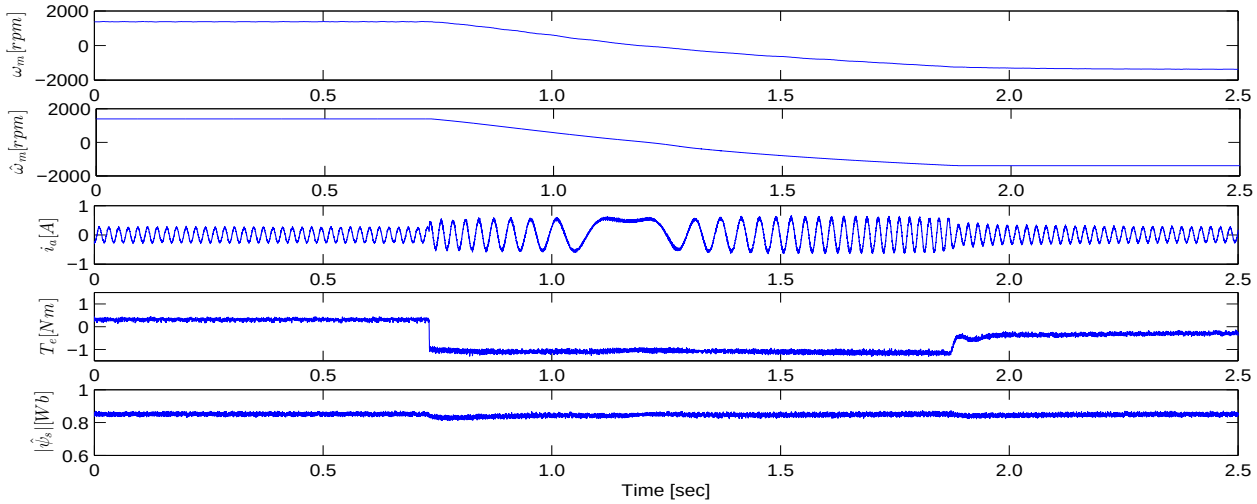

Fig. 6. Experimental waveforms of measured speed, estimated speed, stator current, estimated torque, and estimated stator flux during rated speed (1382rpm) reversal condition with a constant load torque of 0.35Nm.

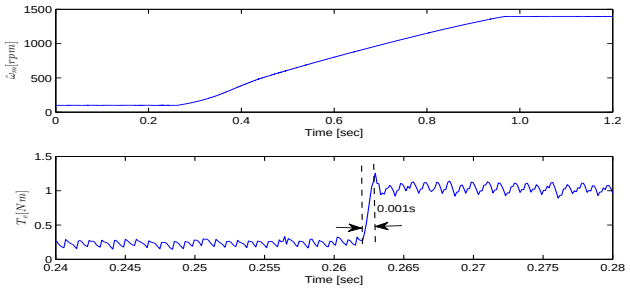

Fig. 7. Experimental torque step response.

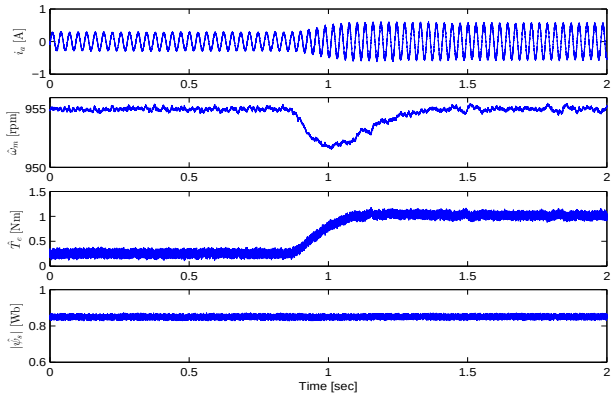

Fig. 8. Experimental waveforms of stator current, estimated speed, electromagnetic torque, and stator flux at 955rpm (100rad/s) under full-load disturbance.

before and after added load are 3.2% and 2.55%, respectively. The load torque which is dependent on speed is changed manually. This is why the torque response is a bit slower. It is also seen that, there is a very small dip in the speed response before compensation. However, no dip is observed in the stator flux response and, therefore, the torque and flux are completely decoupled. Thus, the proposed sensorless drive is robust against load disturbance.

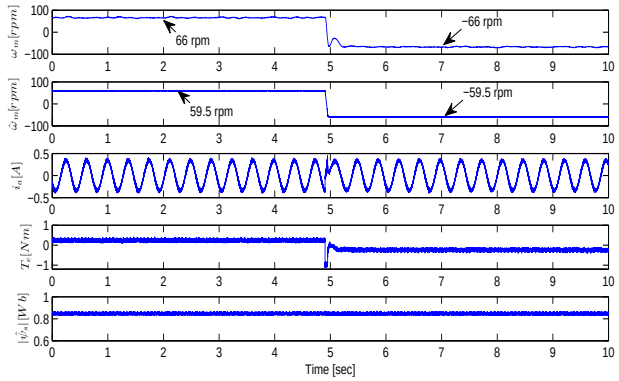

(a)

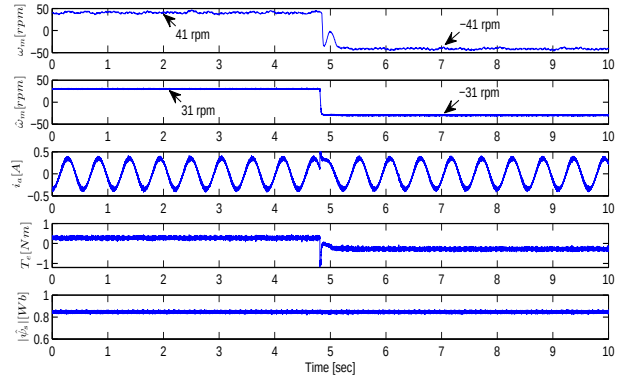

(b)

Fig. 9. Experimental waveforms at low speed reversal using CM based EKF. (a) ±2Hz (60rpm) and (b) ±1Hz (30rpm).

Fig. 9 shows the low speed performance of the proposed sensorless FS-PTC system. The machine is operated at 60rpm (±2Hz) and 30rpm (±1Hz%) in either direction of operating frequencies, and the average measured speed errors are 10.09%

and 32.26%, respectively, which are too high. The THDs of stator currents are 2.13% and 3.7% corresponding to the speed of 60rpm and 30rpm, respectively. It is seen that current model based speed estimator is producing high speed error at lower speeds even though the currents THDs are very good. Moreover, it is quite impossible to estimate zero speed using rotor current model. After many tests, it is observed that the speed response is good when the command speed is greater than $\pm$2Hz which is 4% of rated speed. However, for normal operation, within the range $\pm 2\text{Hz} < \omega_m \leq \pm 50\text{Hz}$, the estimated torque and stator flux responses are still very good, and the system is stable.

In order to reduce the speed error at lower speeds, the open-loop voltage model based EKF is used. The machine is operated again at 60rpm ($\pm$2Hz) and 30rpm ($\pm$1Hz); the waveforms are presented in Fig. 10. It is seen that the speed errors are reduced to 3.36% and 8.33% corresponding to the speed of 60rpm and 30rpm, respectively. The THDs of stator currents are increased to 6.69% and 10.08%, respectively and, therefore, the torque and flux ripples are increased. However, these ripples and current THDs are still acceptable at lower speeds considering improved speed response. The adjustable speed range of the proposed control system is increased by $\pm$1Hz compared with the rotor current model based EKF. Hence, the adjustable speed range of the proposed control system, for normal operation, is $\pm 1\text{Hz} < \omega_m \leq \pm 50\text{Hz}$. After many tests, it was observed that the speed deviation increases rapidly below the adjustable speed range.

The steady state performance of the proposed control system below adjustable speed range is tested for 1rpm with 50% of rated load, and the responses are presented in Fig. 11. Firstly, the measured speed is filtered using a low-pass filter, then it is compared with the estimated speed. The percentages of speed errors $\Delta\omega$ are shown in Fig. 12. For easy understanding and clear information, the percentage of average speed errors, one average value of every 1k data points from the source, are plotted in the Fig. 12. The calculated average speed error for the whole duration of 10sec is 42.18%, which is very high. It is because very low and variable switching frequency characteristics of the FS-PTC strategy. However, the controller produces constant stator flux and good torque waveforms, which indicate the system is stable. The estimated speed is also more accurate, and thus the prediction model is completely free from speed estimation error.

Fig. 13 shows the effects of transition between CM and VM in EKF; this is done by changing rotor speed from 100rpm to 50rpm. It is seen that there is no significant transient in the stator flux, but the estimated torque for VM is a bit higher due to the variation of rotor speed. However, the transient responses of speed and torque are not very good. Since, the speed is very low, it is generally acceptable.

The parameter sensitivity of the proposed sensorless FS-PTC is also investigated at $\pm$60rpm, and shown in Fig. 14. Since, the most critical parameter of the VM is stator resistance and its change greatly influences the control performance at lower speeds, step change of stator resistance from 100%R_s to 130%R_s is applied in both directions of low operating frequency. The average deviation in speed is very small; it

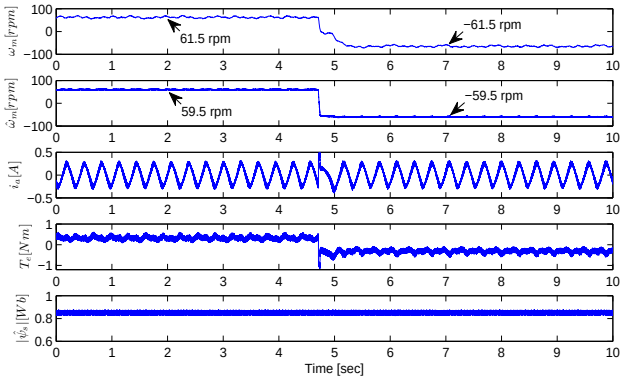

(a)

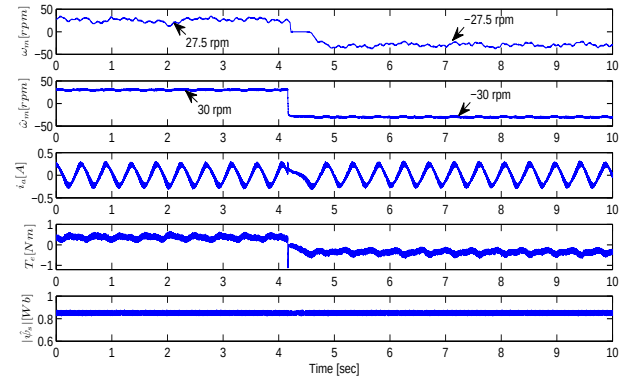

(b)

Fig. 10. Experimental waveforms at low speed reversal using VM based EKF. (a) $\pm$2Hz (60rpm) and (b) $\pm$1Hz (30rpm).

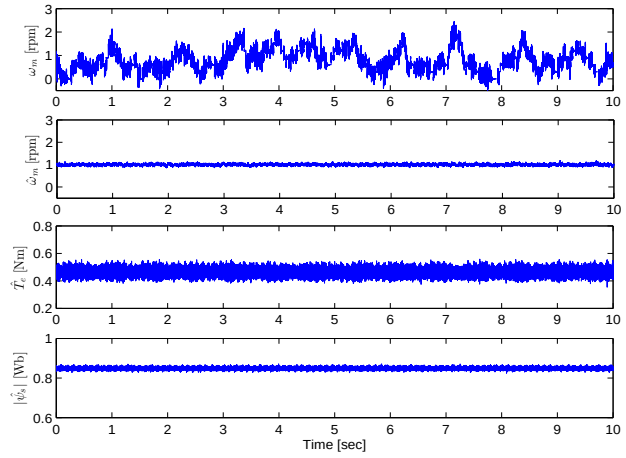

Fig. 11. Experimental waveforms at very low speed (1rpm).

is about 6.5%. It is also seen that the torque is a bit sensitive. However, the stator flux is completely insensitive to the stator resistance variations.

Some tests have also been carried out to confirm the effectiveness of the proposed sensorless control system in the field weakening region. Fig. 15 shows the dynamic performance of the proposed control system in the field weakening region in step speed command from 1rpm to 300% of new rated speed. The torque is constant at its maximum value, as expected, in

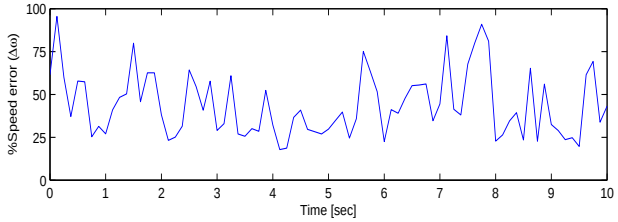

Fig. 12. Experimental percentage steady state speed errors at 1rpm.

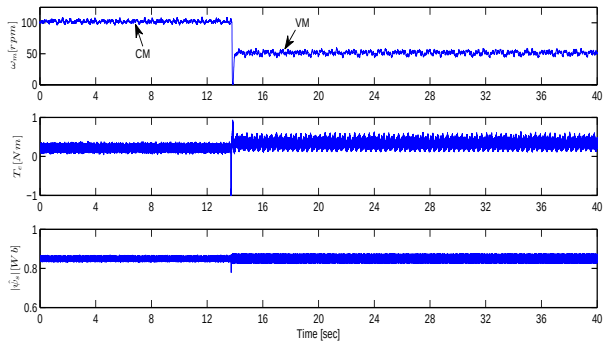

Fig. 13. Experimental waveforms of the effects of transition between CM and VM.

the region I (up to 760rpm), where the stator flux is constant at its nominal value and the stator current is maximum. In the region II (760rpm to 1495rpm), both the stator voltage and the stator current are equal to the limit values, and the stator flux decreases, as expected, to keep the back emf constant. Thus, the maximum torque control is achieved. It can be noted that, the torque decreases from its maximum value as the speed increases further, which keeps the delivered power to the load constant. Once the speed enters into the region III (higher than 1495rpm), the stator current and thus the torque decrease which are also expected, since the available dc link voltage is not sufficient to inject the required maximum current. The vertical dash-dotted lines separate the aforementioned three different regions of operation of the IM. It is also seen that there is a delay between measured and estimated speeds at transient; it is due to the effect of speed quantization error. It is particularly important to note that, the controller is capable of estimating the speed properly in the whole speed range with smooth transition among the field weakening regions and the constant torque region.

VIII. Conclusions

An improved prediction model is proposed for sensorless FS-PTC strategy using EKF and verified by simulation and experiment. Depending on the reference speed, either rotor flux or stator flux is estimated by EKF, then the other one is estimated using the simple relationship between stator and rotor flux. The proposed prediction model uses the estimated currents instead of measured currents and thus the current THD is reduced compared with the conventional FS-PTC where measured currents are directly applied to the prediction model. The estimated speed is also free from noise and thus

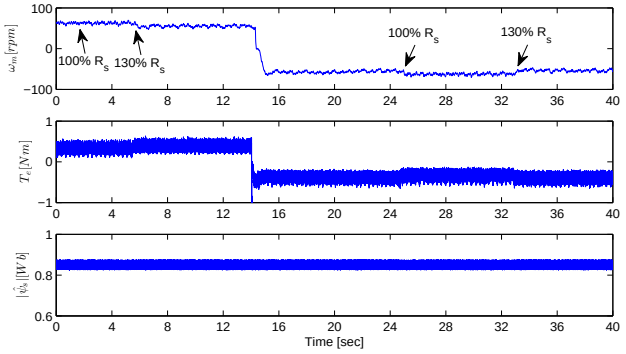

Fig. 14. Stator resistance sensitivity of the voltage model based flux estimator.

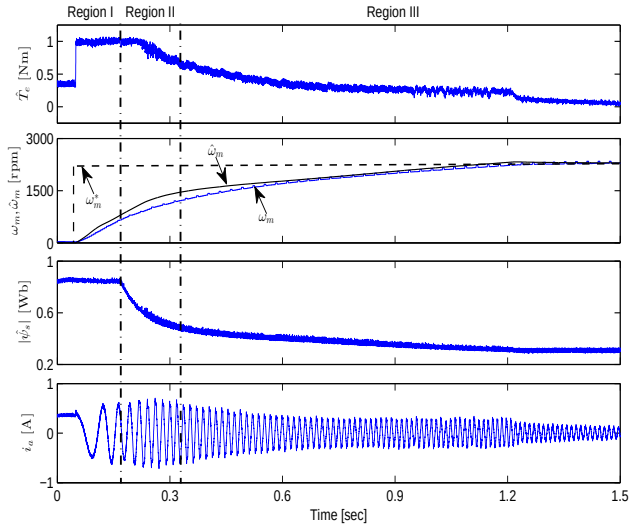

Fig. 15. Experimental dynamic behavior of the machine in the field weakening region in step speed command.

the prediction model is more accurate. Same elements of covariance matrices are considered throughout the experiments; this also enhances the reliability of the control system.

The experimental results show that the proposed sensorless FS-PTC yields very good speed response in a very wide speed range, and the system is completely stable. Since the THD of stator current is less, excellent torque and flux responses are achieved. However, current THD is a bit higher for voltage model, which is generally acceptable considering improved speed response at low speed. This higher current THD corresponds to the lower and variable switching frequency of PTC strategy. It is also investigated that the proposed controller is robust against load disturbance and parameter uncertainty.

In the field weakening region, the controller is well capable of estimating the speed accurately. Also, there is no transient in the estimated torque and flux, when the speed enters from one region to another.

The performance of the proposed controller can be improved further by using an optimized algorithm of EKF which will reduce the control execution time. In that case, the voltage model can be modified by compensating dc offset and drift problems. Hence, the performance at higher speeds in terms

of torque and flux ripples will be comparable with the rotor model based sensorless control strategy.

REFERENCES

[1] S. Kouro, P. Cortes, R. Vargas, U. Ammann, and J. Rodriguez, "Model predictive control–a simple and powerful method to control power converters," *IEEE Trans. Ind. Electron.*, vol. 56, no. 6, pp. 1826–1838, Jun. 2009.

[2] J. Rodriguez, M. P. Kazmierkowski, J. R. Espinoza, P. Zanchetta, H. Abu-Rub, H. A. Young, and C. A. Rojas, "State of the art of finite control set model predictive control in power electronics," *IEEE Trans. Ind. Inf.*, vol. 9, no. 2, pp. 1003–1016, May 2013.

[3] J. H. Lee, "Model predictive control: Review of the three decades of development," *Int. J. Contr. Autom. Syst.*, vol. 9, no. 3, pp. 415–424, 2011.

[4] J. Rodriguez and P. Cortes, *Predictive control of power converters and electrical drives*. New York, Wiley, Mar. 2012, pp. 31–35.

[5] C. A. Rojas, J. Rodriguez, F. Villarroel, J. R. Espinoza, C. A. Silva, and M. Trincado, "Predictive torque and flux control without weighting factors," *IEEE Trans. Ind. Electron.*, vol. 60, no. 2, pp. 681–690, Feb. 2013.

[6] R. Kennel, J. Rodriguez, J. Espinoza, and M. Trincado, "High performance speed control methods for electrical machines: An assessment," *in Proc. IEEE Int. Conf. Ind. Tech.*, Mar. 2010, pp. 1793–1799.

[7] I. M. Alsofyani and N.R.N. Idris, "A review on sensorless techniques for sustainable reliablity and efficient variable frequency drives of induction motors," *Renewable and Sustainable Energy Reviews*, vol. 24, pp. 111–121, Aug. 2013.

[8] J. Holtz, "Sensorless control of induction motor drives," *Proceedings of the IEEE*, vol. 90, no. 8, pp. 1359–1394, Aug. 2002.

[9] S. A. Davari, D. A. Khaburi, F. Wang, and R. M. Kennel, "Using full order and reduced order observers for robust sensorless predictive torque control of induction motors," *IEEE Trans. Power Electron.*, vol. 27, no. 7, pp. 3424–3433, Jul. 2012.

[10] T.-S. Kwon, M.-H. Shin, and D.-S. Hyun, "Speed sensorless stator flux-oriented control of induction motor in the field weakening region using Luenberger observer," *IEEE Trans. Ind. Electron.*, vol. 20, no. 4, pp. 864–869, Jul. 2005.

[11] M. Barut, S. Bogosyan, and M. Gokasan, "Speed-sensorless estimation for induction motors using extended Kalman filters," *IEEE Trans. Ind. Electron.*, vol. 54, no. 1, pp. 272–280, Feb. 2007.

[12] Y.-R. Kim, S.-K. Sul, and M.-H. Park, "Speed sensorless vector control of induction motor using extended Kalman filter," *IEEE Trans. Ind. Appl.*, vol. 30, no. 5, pp. 1225–1233, Sep./Oct. 1994.

[13] F. Wang, Z. Chen, P. Stolze, J-F. Stumper, J. Rodrguez, and R. Kennel, "Encoderless finite-state predictive torque control for induction machine with a compensated MRAS," *IEEE Trans. Ind. Inf.*, vol. 10, no. 2, pp. 1097–1106, May 2014.

[14] J. Guzinski and H. Abu-Rub, "Speed sensorless induction motor drive with predictive current controller," *IEEE Trans. Ind. Electron.*, vol. 60, no. 2, pp. 699–709, Feb. 2013.

[15] F. Wang, Z. Zhang, S. A. Davari, R. Fotouhi, D. A. Khaburi, J. Rodrguez, and R. Kennel, "An encoderless predictive torque control for an induction machine with a revised prediction model and EFOSMO," *IEEE Trans. Ind. Electron.*, vol. 61, no. 12, pp. 6635–6644, Dec. 2014.

[16] Zhong-gang Yin, Chang Zhao, Yan-Ru Zhong, and Jing Liu, "Research on robust performance of speed-sensorless vector control for the induction motor using an interfacing multiple-model extended Kalman filter," *IEEE Trans. Power Electron.*, vol. 29, no. 6, pp. 3011–3019, Jun. 2014.

[17] K. L. Shi, T. F. Chan, Y. K. Wong, and S. L. Ho, "Speed estimation of an induction motor drive using an optimized extended Kalman filter," *IEEE Trans. Ind. Electron.*, vol. 49, no. 1, pp. 124–133, Feb. 2002.

[18] S. Blognani, L. Tubiana, and M. Zigliotto, "Extended Kalman filter tuning in sensorless PMSM drives," *IEEE Trans. Ind. Appl.*, vol. 39, no. 6, pp. 1741–1747, Nov./Dec. 2003.

[19] F. Alonge, F. D'Ippolito, and A. Sferlazza, "Sensorless control of induction-motor drive based on robust Kalman filter and adaptive speed estimation," *IEEE Trans. Ind. Electron.*, vol. 61, no. 3, pp. 1444–1453, Mar. 2014.

[20] M. Habibullah and D.D.C. Lu, "Encoderless FS-PTC for induction motor with extended Kalman filter," *in Proc. Australasian Univ. Power Eng. Conf. (AUPEC)*, Sep./Oct. 2014, pp. 1–5.

[21] P. Cortes, J. Rodriguez, C. Silva, and A. Flores, "Delay compensation in model predictive current control of a three-phase inverter," *IEEE Trans. Ind. Electron.*, vol. 59, no. 2, pp. 1323–1325, Feb. 2012.

[22] J. M. D. Murphy and F. G. Turnbull, *Power electronic control of ac motors*. New York: Pergamon, 1988, pp. 284–287.

[23] S-H Kim and S-K Sul, "Maximum torque control of an induction machine in the field weakening region," *IEEE Trans. Ind. Appl.*, vol. 31, no. 4, pp. 787–794, Jul./Aug. 1995.

[24] M. Mengoni, L. Zarri, A. Tani, G. Serra, and D. Casadei, "Stator flux vector control of induction motor drive in the field weakening region," *IEEE Trans. Power Electron.*, vol. 23, no. 2, pp. 941–949, Mar. 2008.

[25] H. W. Van Der Broeck, H-C. Skudelny, and G. V. Stanke, "Analysis and realization of a pulsewidth modulator based on voltage space vectors," *IEEE Trans. Ind. Appl.*, vol. 24, no. 1, pp. 142–150, Jan./Feb. 1988.

[26] P. Vas, *Vector control of ac machines*. Oxford, U.K.: Clarendon, 1990, pp. 124–126.

Md. Habibullah (S'13) received the B.Sc. and M.Sc. degrees in Electrical and Electronic Engineering from Khulna University of Engineering & Technology (KUET), Bangladesh in 2008 and 2012, respectively. He is currently pursuing his PhD degree in the School of Electrical and Information Engineering at The University of Sydney, Sydney, Australia. He is also a faculty member of the Department of Electrical and Electronic Engineering at KUET, Khulna, Bangladesh. His research interests include power electronics and control applications to electrical drives.

Dylan Dah-Chuan Lu (S'00 M'04 SM'09) received his B.Eng. (Hons.) and Ph.D. degrees in Electronic and Information Engineering from The Hong Kong Polytechnic University, Hong Kong in 1999 and 2004 respectively.

In 2003, he joined Power^{e}Lab Ltd. as a Senior Design Engineer. His major responsibilities included project development and management, circuit design, and contribution of research in power electronics. In 2006, he joined the School of Electrical and Information Engineering, The University of Sydney, Australia, where he is currently a Senior Lecturer. From July 2013 to December 2013, he was with the University of Hong Kong as a visiting Associate Professor. He is the author and co-author of over 120 papers in the areas of power electronics and engineering education. He has two patents on efficient power conversion. His current research interests include power electronics circuits and control for efficient power conversion, lighting, renewable electrical energy systems, microgrids, motor drive and power quality improvement, and engineering education.

Dr. Lu is a member of the Institute of Engineers Australia. He presently serves as an Associate Editor of the IET Renewable Power Generation and the International Journal of Electronics. He also served as a Guest Editor of the IEEE Transactions on Industrial Electronics; special issue on Power Converters, Control and Energy Management for Distributed Generation in 2014.